Dentomaxillofacial Radiology (2017) 46, 20160107

birpublications.org/dmfr

RESEARCH ARTICLE

Detection of vertical root fractures in intact and endodontically treated premolar teeth by designing a probabilistic neural network: an *ex vivo* study

[1]Masume Johari, [1]Farzad Esmaeili, [2]Alireza Andalib, [1]Shabnam Garjani and [3]Hamidreza Saberkari

[1]Department of Oral and Maxillofacial Radiology, Faculty of Dentistry, Dental and Periodontal Research Center, Tabriz University of Medical Sciences, Tabriz, Islamic Republic of Iran; [2]Department of Electrical Engineering, Tabriz Branch, Islamic Azad University, Tabriz, Islamic Republic of Iran; [3]Department of Electrical Engineering, Sahand University of Technology, Tabriz, Iran

Objectives: Detection of vertical root fractures (VRFs) in their initial stages is a crucial issue, which prevents the propagation of injury to the adjacent supporting structures. Designing a suitable neural network-based model could be a useful method to diagnose the VRFs. The aim of this study was to design a probabilistic neural network (PNN) to diagnose the VRFs in intact and endodontically treated teeth of periapical and CBCT radiographs. Also, we have compared the efficacy of these two imaging techniques in the detection of VRFs.

Methods: A total of 240 radiographs of teeth (120 radiographs of teeth with no VRFs and 120 teeth with vertical fractures, with half of the teeth in each category treated endodontically and the remaining half intact, *i.e.* not endodontically treated) were used in 3 groups for training and testing of the neural network as follows: Group 1, 180/60; Group 2, 120/120; and Group 3, 60/180. First, Daubechies 3 wavelet was applied to acquire the image analysis coefficients on two planes; then Gabor filters were used to extract the image characteristics, which were used to educate the PNN. The designed neural network was able to diagnose and classify teeth with and without VRFs. In addition, in order to determine the best training and test sets in the network, the variance of the function of network changes was manipulated at a range of 0–1 and the results were assessed in terms of the parameters evaluated, including sensitivity, specificity and accuracy.

Results: In the periapical radiographs, the maximum accuracy, sensitivity and specificity values in the three groups were 70.00, 97.78 and 67.7%, respectively. These values in the CBCT images were 96.6, 93.3 and 100%, respectively, at the variance change range of 0.1–0.65.

Conclusions: The designed neural network can be used as a proper model for the diagnosis of VRFs on CBCT images of endodontically treated and intact teeth; in this context, CBCT images are more effective than similar periapical radiographs. Limitations of this study are the use of sound one-rooted premolar teeth without carious lesions and dental fillings and not simulating the adjacent anatomic structures. Further *in vitro* work using a full-skull simulation for CBCT and skin/bone simulation is needed.

Dentomaxillofacial Radiology (2017) **46**, 20160107. doi: 10.1259/dmfr.20160107

Cite this article as: Johari M, Esmaeili F, Andalib A, Garjani S, Saberkari H. Detection of vertical root fractures in intact and endodontically treated premolar teeth by designing a probabilistic neural network: an *ex vivo* study. *Dentomaxillofac Radiol* 2017; **46**: 20160107.

Keywords: root fracture; detection; neural network; image processing

Correspondence to: Dr Masume Johari. E-mail: khatoonm87@yahoo.com

The Dental and Periodontal Research Center, Tabriz University of Medical Sciences, is the main funder of this work.

Received 16 March 2016; revised 21 October 2016; accepted 25 October 2016

Introduction

Vertical root fractures (VRFs) are rare events that mainly occur in endodontically treated teeth that have received posts without receiving a crown and are subject to trauma.[1] In such cases, the width of the fracture plane increases over time.[2] Early diagnosis of root fractures in their initial stages prevents the propagation of injury to the adjacent supporting structures.[3]

The ability of intraoral images to detect root fractures depends on the X-ray beam angulation and the amount of separation of the fractured segments.[4] If the X-ray beam is parallel to the plane of the fracture, a single and very distinct radiolucent line will be evident on the root anatomy. However, if the X-ray beam is oblique relative to the plane of the fracture, the fracture line will be visible as a single indistinct line or as two lines that converge on the mesial and distal surfaces of the root.[5]

In recent years, CBCT imaging technique with a high resolution and varying sensitivity and specificity has been widely used for the diagnosis of VRFs. This imaging technique allows the operator to evaluate the fracture in different planes. However, various factors including artefacts resulting from the root canal obturation materials, metallic posts and the absence of separation of fractured segments have made it a challenge to diagnose such fractures with use of this imaging technique.[6–8]

An artificial neural network is a pattern for processing data, which is constructed using neural networks such as the human brain.[9] The key element of this pattern is the new structure of its data-processing system, which is composed of a large number of elements (neurons) with strong internal connections that operate harmoniously to solve specific problems.[10] In such networks, programming science is used to design a data structure than can function as a neuron. Such a data structure is referred to as a node. Then, this network is trained by creating connections between these nodes and application of a training algorithm to the network. In a neural network, the nodes have two states of active (on or 1) and inactive (off or 0) and each synapse or connection between the nodes has a weight. Synapses with a positive weight stimulate or activate the next inactive node and synapses with a negative weight inactivate or inhibit the next node (if it is active).[11] Generally, there are three neuron layers in neural networks, including (1) the input layer, which is responsible for receiving raw data; (2) the hidden layer, whose performance is determined by inputs and the weight of their connections with the hidden layers; and (3) the output layer, whose performance depends on the activity of the hidden layer and the weight of the relationship between the hidden layer and the output layer.[12]

In the present study, a probabilistic neural network (PNN) was designed to diagnose the VRFs in intact and endodontically treated teeth of periapical and CBCT radiographic images. First, Daubechies 3 wavelet transform[13] was applied to acquire the image coefficients in two states. Then, Gabor filters[14] were used to extract image characteristics, which were used to train the PNN. The neural network designed this way was able to diagnose and categorize teeth with and without VRFs. Furthermore, the variable of the function of changes in the network was manipulated at a range of 0–1 in order to determine the best training and test sets in the network, followed by evaluation of sensitivity, specificity and accuracy as the study parameters.

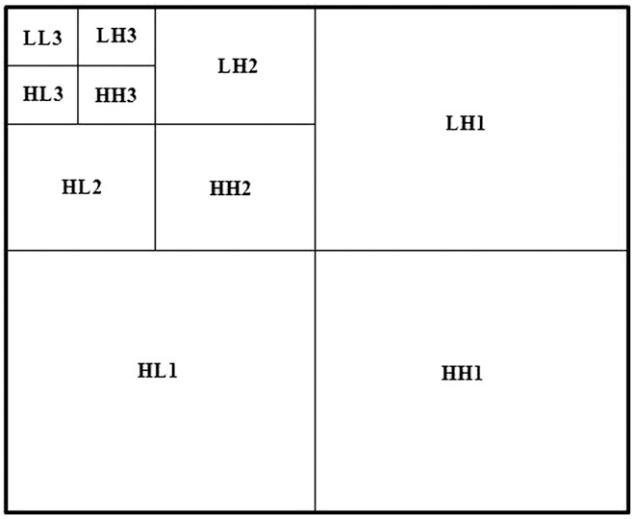

Figure 1 The stages of the application of Daubechies 3 wavelet transform to the input image.

Methods and materials

Preparation of teeth and the imaging protocol

The teeth under study consisted of extracted sound one-rooted premolars with no carious lesions. The teeth were rinsed and cleaned with brushes and stored in formalin. Then, they were evaluated under a microscope at ×20 for the presence or absence of any fractures. After selection

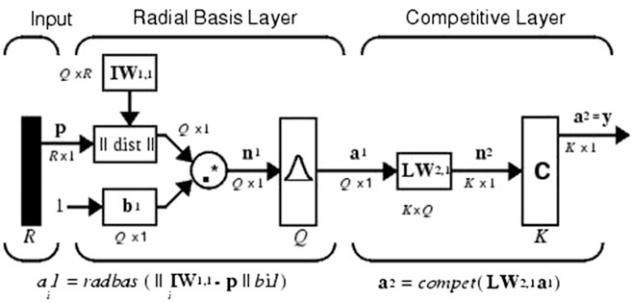

Figure 2 The structure of the probabilistic neural network: *a*, the output vector in radial basis; *b*, the amount of bias; *c*, the output vector in the competitive layer; *d*, the input vector in the competitive layer; *k*, the number of classes (with fracture and without fracture); *M*, the weight matrix in the competitive layer; *n*, the input vector in radial basis; *p* vector, the input variable; *Q*, the training vector; *R*, the number of variables; *W*, the weight matrix.

Table 1 Different tooth groups for training and testing of the neural network

	Train				*Test*				
Tested groups	*Fx endo*	*Fx non-endo*	*Non-fx endo*	*Non-fx non-endo*	*Fx endo*	*Fx non-endo*	*Non-fx endo*	*Non-fx non-endo*	*Total*
Group 1	45	45	45	45	15	15	15	15	240
Group 2	30	30	30	30	30	30	30	30	240
Group 3	15	15	15	15	45	45	45	45	240

Fx, fractured.

of 240 teeth, half of them ($n = 120$) underwent endodontic procedures and the remaining 120 teeth were left intact. The tooth crowns were removed at 2 mm apical to the Cementoenamel Junction. The root canals were prepared with the ProTaper® (Dentsply Maillefer, Ballaigues, Switzerland) rotary system up to #F5 and obturated with ProTaper #F5 gutta percha points. The teeth were fixed in an acrylic resin box using 1-mm-thick wax. 60 endodontically treated teeth and 60 intact teeth were connected to a universal testing machine at a 60° angle and received a force until they fractured. Then, the teeth were retrieved from the wax and re-evaluated under microscope at ×20 to make sure of the presence of fracture. All the 240 teeth were assigned to 3 groups as follows: Group 1, 180/60 (60 training data and 180 test data); Group 2, 120/120 (120 training data and 120 test data); and Group 3, 60/180 (180 training data and 60 test data) for the education and testing of the neural network.

Kodak 2200 Intraoral X-ray system was used in this study. The system uses a high-frequency generator Alternating Current. The X-ray beams were irradiated using a round collimator at 60 kVp and 7 mA for 0.08 s. The film–focus distance was 24 cm and the film–object distance was 1 cm.

An RVG sensor was used for periapical imaging (Kodak RVG 5100 with 14-lp mm^{-1} image resolution), with the faciolingual aspect parallel to the sensor, and the images were saved in the Joint Photographic Experts Group format.

To obtain CBCT images, a conical X-ray beam was used with a 1920 × 1536-pixel flat-panel detector, with 360° rotation. The examination with NewTom VGi (QR SRL Company, Verona, Italy) was performed at 4.71 mA and 110 kVp with scan time of 3.6 s. The slice thickness was 1 mm. The primary and secondary reconstructions were performed with NNT viewer v. 2.2.1 (Quantitive Radiology, Verona, Italy).

Feature extraction from the radiographs using wavelet transform

In the present study, Daubechies 3 wavelet transform[13] was first applied to extract the important data in the images, especially at image margins. Figure 1 demonstrates the procedures used to apply the wavelet to the input image. In this figure, H and L are the high- and low-pass filters, respectively, and HH means the application of high-pass filter at both vertical and horizontal dimensions to the image. Application of Daubechies 3 wavelet resulted in the acquisition of image analysis coefficients on two states.

In the second step, the wavelet coefficients were used to extract the specificity vector using the Gabor filters.[14] These filters can be used to optimize the display of a signal in the time and frequency fields simultaneously. The Gabor filters used for processing of images are two-dimensional and each filter has a definitive frequency and direction. To acquire the feature vector, first the disintegration coefficients resulting from Daubechies 3 wavelet were divided into eight different directions and then, eight Gabor filters, with the same frequency and each in one direction, were applied to it. Finally, for each pixel of the image, the direction in which the output application of the Gabor filter had the highest value was selected as the indicator of that point of the image on the specificity vector and this vector was used for training the neural network. More details of the Gabor filters are provided in Appendix A.

Designing the probabilistic neural network to train the extracted features

The PNN consists of three layers (Figure 2); when an input vector is applied to the network, the first layer calculates the distance between the input vector and the training inputs, providing a vector, the elements of which determine the distance between the input and the training data. This layer consists of a radial basis layer, whose conversion function (Radbas) is a Gaussian function $f(x) = e^{-x^2/\sigma^2}$, in which σ is the function variance. The output of this layer (Figure 2) is a bell-shaped function, in which the extension of the function is controlled by the σ parameter. The output of Radbas function is considered an input for the second layer, which is a competitive layer. In this layer, the maximum value of probabilities is selected from the probability vector and an output of 1 is created for it and an output of 0 is created for all the other probabilities. As a result, this layer is divided into two groups of teeth with and without fractures.

Training and testing of the neural network was carried out with the use of the specificity vector acquired from the Gabor filters for both teeth with and without root fractures, and endodontically and not endodontically treated teeth, with the use of periapical and CBCT radiographic images. Test and training data were classified into three groups based on Table 1. Each group consisted of teeth with and without root fractures. In addition, in order to determine the best training and test sets in the network, the Gaussian function variance σ was manipulated at 0–1 range and the results were evaluated in terms of evaluation parameters such as sensitivity specificity and accuracy. The model used for

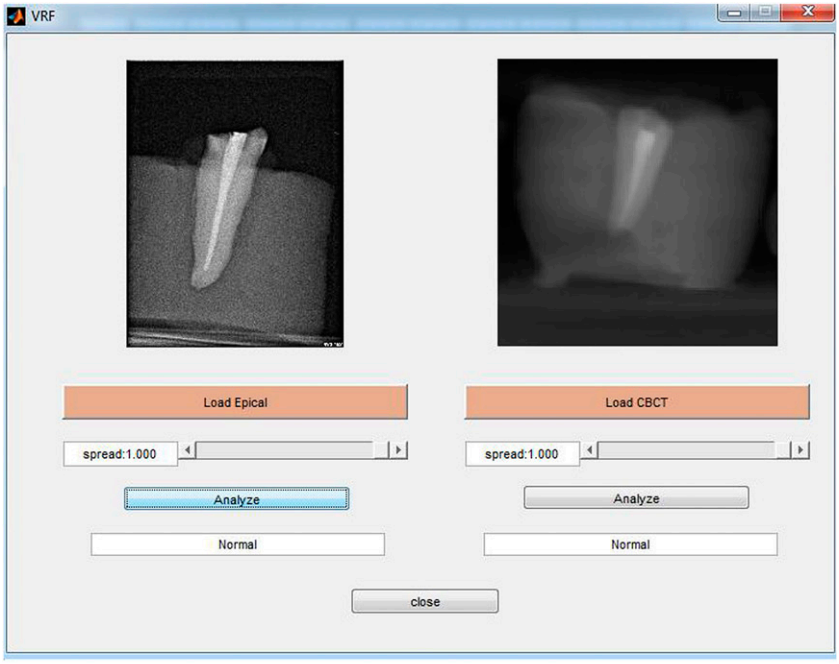

(a)

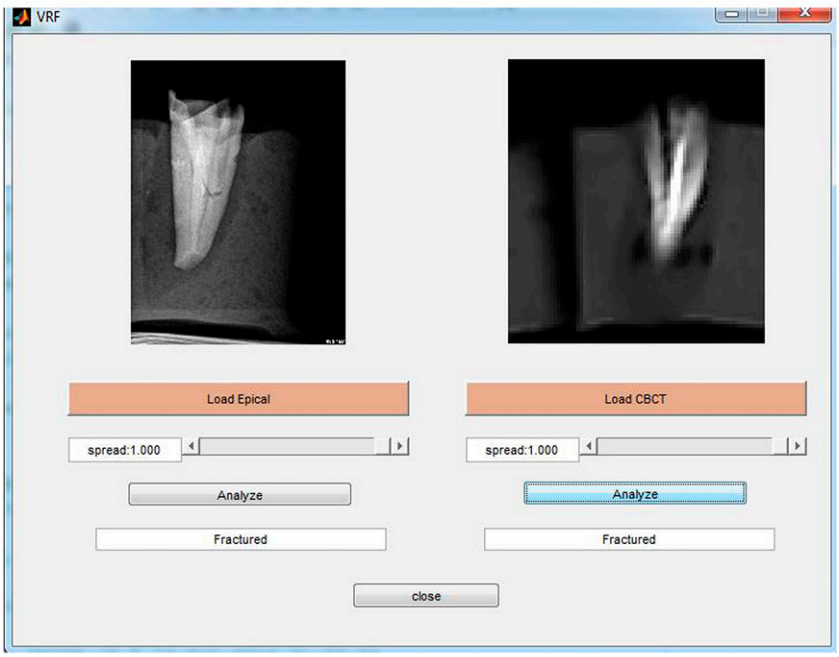

(b)

Figure 3 The software package designed for the diagnosis of vertical fracture of the root on periapical and CBCT radiographic images: (a) normal root and (b) root with fracture.

the diagnosis of root fractures in teeth was designed in the graphic milieu of the MATLAB® software program (MathWorks®, Natick, MA) as shown in Figure 3. The designed software was able to load the periapical and CBCT images separately, it made it possible for the operator to change the sigma parameter manually from 0 to 1 and it made it possible to observe the output result. The output report was presented to the operator in the form of a message, which might have consisted of the normality of the root (Figure 3a) or of VRF (Figure 3b). It should be mentioned that the raw periapical and CBCT radiographies have been compressed in this study in order to detect the edges of the images, including fractures, more clearly. The dimension of the periapical and CBCT radiographies before/after compression are $160 \times 120/16 \times 12$, respectively.

Table 2 Accuracy, sensitivity and specificity values of the test data in Group 1 (training data = 180, test data = 60) for periapical (PA)/CBCT radiographs

	Fx (n = *30*)		*Non-fx* (n = *30*)		*Accuracy (%)*		*Sensitivity (%)*		*Specificity (%)*	
Variance of function	*PA*	*CBCT*	*PA*	*CBCT*	*PA*	*CBCT*	*PA*	*CBCT*	*PA*	*CBCT*
0.05	21	22	20	30	68.33	86.66	70.00	73.33	67.74	100
0.1	21	28	20	30	68.33	96.66	70.00	93.33	67.74	100
0.15	21	28	20	30	68.33	96.66	70.00	93.33	67.74	100
0.2	20	28	17	30	61.67	96.66	66.67	93.33	60.61	100
0.25	20	28	17	30	61.67	96.66	66.67	93.33	60.61	100
0.3	22	28	17	30	65.00	96.66	73.33	93.33	62.86	100
0.35	22	28	16	30	63.33	96.66	73.33	93.33	61.11	100
0.4	24	28	15	30	65.00	96.66	80.00	93.33	61.54	100
0.45	24	28	14	30	63.33	96.66	80.00	93.33	60.00	100
0.5	24	28	14	30	63.33	96.66	80.00	93.33	60.00	100
0.55	25	28	14	30	65.00	96.66	83.33	93.33	60.98	100
0.6	27	28	14	30	68.33	96.66	90.00	93.33	62.79	100
0.65	27	28	14	30	68.33	96.66	90.00	93.33	62.79	100
0.7	28	26	14	30	70.00	93.33	93.33	86.66	63.64	100
0.75	28	26	11	30	65.00	93.33	93.33	86.66	59.57	100
0.8	28	26	10	30	63.33	93.33	93.33	86.66	58.33	100
0.85	28	24	10	30	63.33	90.00	93.33	80.00	58.33	100
0.9	28	23	10	30	63.33	88.33	93.33	76.66	58.33	100
0.95	28	20	8	30	60.00	88.33	93.33	66.66	56.00	100
1	28	20	7	30	58.33	88.33	93.33	66.66	54.90	100

Fx, fractured.

Statistical analysis

The performance of the designed neural network was evaluated with the use of diagnostic parameters (sensitivity and specificity). Sensitivity indicates the performance of the neural network in the diagnosis of fractures. Specificity shows the performance of the network in correct determination of the number of teeth without fracture. Accuracy is defined as the ratio of correct diagnosis over the whole data as shown below:

$$\text{Accuracy} = \frac{\text{TP} + \text{TN}}{\text{TP} + \text{TN} + \text{FP} + \text{FN}}. \quad (1)$$

In Equation (1), each parameter, FP, FN, TP and TN, could be defined as follows:

FP (false positive): number of teeth without fractures diagnosed as fracture mistakenly through the algorithm

FN (false negative): number of teeth with fractures, which were not considered as a fracture by the algorithm

TP (true positive): number of teeth with fractures that were considered as fracture using the algorithm

Table 3 Accuracy, sensitivity and specificity values of the test data in Group 2 (training data = 120, test data = 120) for periapical (PA)/CBCT radiographs

	Fx (n = *60*)		*Non-fx* (n = *60*)		*Accuracy (%)*		*Sensitivity (%)*		*Specificity (%)*	
Variance of function	*PA*	*CBCT*	*PA*	*CBCT*	*PA*	*CBCT*	*PA*	*CBCT*	*PA*	*CBCT*
0.05	35	44	39	60	61.67	86.67	58.33	73.33	62.50	100
0.1	35	54	38	60	60.83	95.00	58.33	90.00	61.40	100
0.15	35	54	38	60	60.83	95.00	58.33	90.00	61.40	100
0.2	35	54	39	60	61.67	95.00	58.33	90.00	62.50	100
0.25	37	54	41	60	65.00	95.00	61.67	90.00	66.07	100
0.3	36	54	37	60	60.83	95.00	60.00	90.00	61.02	100
0.35	40	54	36	60	63.33	95.00	66.67	90.00	62.50	100
0.4	44	54	33	60	64.17	95.00	73.33	90.00	61.97	100
0.45	49	54	29	60	65.00	95.00	81.67	90.00	61.25	100
0.5	49	54	27	60	63.33	95.00	81.67	90.00	59.76	100
0.55	50	54	26	60	63.33	95.00	83.33	90.00	59.52	100
0.6	52	52	25	60	64.17	93.33	86.67	86.67	59.77	100
0.65	53	52	24	60	64.17	93.33	83.33	86.67	59.55	100
0.7	55	52	21	60	63.33	93.33	91.67	86.67	58.51	100
0.75	55	51	17	60	60.00	92.50	91.67	85.00	56.12	100
0.8	56	51	14	60	58.33	92.50	93.33	85.00	54.90	100
0.85	57	49	13	60	58.33	90.83	95.00	81.67	54.81	100
0.9	57	47	11	60	56.67	89.17	95.00	78.33	53.77	100
0.95	58	45	10	60	56.67	87.50	96.67	75.00	53.70	100
1	58	45	8	60	55.00	87.50	96.67	75.00	52.73	100

Fx, fractured.

Table 4 Accuracy, sensitivity and specificity values of the test data in Group 3 (training data = 60, test data = 180) for periapical (PA)/CBCT radiographs

	Fx (n = 90)		*Non-fx* (n = 90)		*Accuracy (%)*		*Sensitivity (%)*		*Specificity (%)*	
Variance of function	*PA*	*CBCT*	*PA*	*CBCT*	*PA*	*CBCT*	*PA*	*CBCT*	*PA*	*CBCT*
0.05	56	60	44	90	55.56	83.33	62.22	66.67	54.90	100
0.1	56	78	43	90	55.00	93.33	62.22	86.67	54.37	100
0.15	56	78	43	90	55.00	93.33	62.22	86.67	54.37	100
0.2	57	78	45	90	56.67	93.33	63.33	86.67	55.88	100
0.25	59	78	45	90	57.78	93.33	65.56	86.67	56.73	100
0.3	59	78	41	90	55.56	93.33	65.56	86.67	54.63	100
0.35	63	79	40	89	57.22	93.89	70.00	87.78	55.75	100
0.4	66	79	40	89	58.89	93.33	73.33	87.78	56.90	100
0.45	68	79	35	89	57.22	93.33	75.56	87.78	55.28	98.75
0.5	72	79	33	89	58.33	93.33	80.00	87.78	55.81	98.75
0.55	80	79	35	89	63.89	93.33	88.89	87.78	59.26	98.75
0.6	81	79	29	89	61.11	93.33	90.00	87.78	57.04	98.75
0.65	82	79	27	89	60.56	93.33	91.11	87.78	56.55	98.75
0.7	83	79	25	89	60.00	93.33	92.22	87.78	56.08	98.75
0.75	84	79	21	89	58.33	93.33	93.33	87.78	54.90	98.75
0.8	85	78	18	89	57.22	92.78	94.44	86.67	54.14	98.73
0.85	85	77	15	89	55.56	92.22	94.44	85.56	53.13	98.72
0.9	87	77	13	89	55.56	92.22	96.67	85.56	53.05	98.72
0.95	88	77	12	89	55.56	92.22	97.78	85.56	53.01	98.72
1	88	76	8	89	53.33	91.67	97.78	84.44	51.76	98.70

Fx, fractured.

TN (true negative): number of teeth without fractures, which were diagnosed correctly as non-fractured by the algorithm.

Results

Tables 2–4 present the sensitivity, specificity and accuracy values acquired from the suggested algorithm for the test data and for the three groups of data separately for each change in the sigma parameter from 0.05 to 1. The sigma parameter is the same parameter defined in the Gaussian function [the Radbas function $f(x)=e^{-x^2/\sigma^2}$] in the PNN. Change in the sigma parameter in Radbas function leads to change in the slope of the separation boundary of two classes (sound/fracture teeth). By reducing the distance between the weights vector and the inputs, the output of Radbas function is increased. Therefore, the sigma parameter could have a significant impact on correct identification of the data, which is close to the separation boundary of two classes. Choosing high/low amounts of sigma parameter leads to generalization/overfitting issues, respectively.[10]

In Group 1, the maximum accuracy value for periapical radiographs was 70% at $\sigma = 0.7$; however, this value for CBCT images was 96.66% at $\sigma = 0.1$–0.65. Therefore, CBCT images were 1.38 times more accurate than periapical radiographs. The maximum sensitivity value for periapical radiographs in this group was 93.33% at $\sigma = 0.7$–1; this value for CBCT images was similar to that for periapical images (93.33%), but at $\sigma = 0.1$–0.65. In addition, the highest specificity value at low sigma values for periapical radiographs was 67.74% at $\sigma = 0.05$–0.15 and this value was 100% for CBCT images at all the sigma levels.

In Group 2, the maximum accuracy value for periapical radiographs was 65% at $\sigma = 0.45$; this value for CBCT images was 95% at $\sigma = 0.1$–0.55, indicating 1.46 times higher accuracy with CBCT images compared with periapical images. The highest sensitivity value for periapical radiographs in this group was 96.67% at $\sigma =$ 0.95–1; this value for CBCT images was 90% at $\sigma =$ 0.1–0.55. In addition, the maximum specificity value for periapical radiographs was 66.07% at $\sigma = 0.25$; this value for CBCT images was 100% at all the sigma values (similar to specificity values in Group 1).

In Group 3, the maximum accuracy value for periapical radiographs was 63.89% at $\sigma = 0.55$; however, this value for CBCT images was 93.89% at $\sigma = 0.35$% and 93.33% at $\sigma = 0.1$–0.3 and $\sigma = 0.4$–0.75. The maximum sensitivity value for periapical radiographs in this group was 97.78% at $\sigma = 0.95$ and $\sigma = 1$. This

Table 5 The best performance of the designed neural network in each group of periapical (PA) radiographs

PA graphics	*Variance of function*	*Specificity (%)*	*Sensitivity (%)*	*Accuracy (%)*
Group 1	0.05–0.15	63.64	93.33	70.00
Group 2	0.25	66.07	61.67	65.00
	0.45	61.25	81.67	65.00
Group 3	0.55	59.26	88.89	63.89

Table 6 The best performance of the designed neural network in each group of CBCT radiographs

CBCT graphics	*Variance of function*	*Specificity (%)*	*Sensitivity (%)*	*Accuracy (%)*
Group 1	0.1–0.65	100	93.33	96.66
Group 2	1.1–0.55	100	90.00	95.00
Group 3	1.1–0.3	100	86.67	93.33
	0.4–0.75	98.75	87.78	93.33

value for CBCT images was 87.78% at $\sigma = 0.35$–0.75. In addition, the maximum specificity value for periapical radiographs was 59.26% at $\sigma = 0.55$; this value for CBCT images was 100% at $\sigma = 0.05$–0.35.

Tables 5 and 6 summarize the best performance of the algorithm in each group along with the best function variance of the network for periapical and CBCT radiographs. Two important parameters, accuracy and size of the network, are the most important parameters that should be considered when a classifier is designed based on the neural network. In a neural network, the classification error could be reduced by changing the architecture of the network. In the designed PNN, the classification error is reduced by changing the variance of function (sigma parameter). The reason for spacing the variance of function in 20 steps is that we want to find the best ranges of sigma in which the highest amounts of accuracy, sensitivity and specificity are achieved (Tables 5 and 6).

In order to compare the performance of the designed PNN with other state-of-the-art approaches, we have applied the multilayer perceptron (MLP) network and the parameters of accuracy, sensitivity and specificity are calculated as shown in Tables 7 and 8 for periapical and CBCT radiographs, respectively. We should mention that the Gabor filter is applied to the image in eight directions. So, the number of extracted features is 8704, which is a large number. The large number of features leads to the MLP network failing to classify the data correctly. To overcome this problem, we have applied the principle component analysis method.[15] By this modification, the number of extracted features is dropped to 240 in each radiograph. The aforementioned issue is not present in the PNN owing to employment of competitive layer. As can be seen in Tables 7 and 8, even after reducing the number of features, the accuracy, sensitivity and specificity parameters of PNN are higher than that of MLP network in all three groups. However, in terms of time, the MLP algorithm is faster than PNN. The training procedure of MLP network took around 2.14 s, while this is around 3.46 s for PNN.

Discussion

Detection of VRF is a vital clinical problem with subsequent destruction of the adjacent bone. Hence, cases of VRF necessitate extraction of the tooth. With other causes of periradicular chronic inflammatory processes or periradicular cystic lesions, apical root resection suffices. Thus, pre-operative detection of a fracture influences therapeutic strategies.

A PNN was designed in the present study to diagnose the VRFs of periapical and CBCT images in endodontically treated and intact premolars that had no caries. Both types of radiographs are divided into three categories; Group 1: the training data are more than the test data, Group 2: training and test data are equal and Group 3: the amount of test data are higher than the amount of training data. The designed neural network had some advantages compared with other neural networks, including (1) its easy design; (2) accurate classification of training data; and (3) its resistance to noise. Such advantages have made it possible for these neural networks to have many other applications such as classification and regression.[16,17]

It was illustrated that CBCT has a higher sensitivity (88%) and specificity (75%) in comparison with other imaging methods in the detection of the VRFs.[18] Furthermore, clinical results prove that CBCT scans are more accurate in the detection of 0.2- and 0.4-mm VRFs (70 and 90%, respectively) compared with digital radiography (43.3 and 60%, respectively).[19] While the reported sensitivity and specificity for conventional intraoral radiography were 38 and 87%, respectively, sensitivity and specificity of 48 and 89% were achieved through digital radiography.[20]

The neural network was able to make more accurate diagnoses of fractures at high sigma values in periapical radiographs. In this context, in all the three groups, a sensitivity value of over 93% was achieved at the sigma values >0.8, indicating the fact that the designed neural network was able to reach high sensitivity with any amount of training data. However, the correct diagnosis of sound teeth occurred at low sigma levels. The advantage of greater training data, in addition to higher

Table 7 Accuracy, sensitivity and specificity quantities of the test data for periapical (PA) radiographs by applying multilayer perceptron neural network

PA graphics	*Fx*	*Non-fx*	*Accuracy (%)*	*Sensitivity (%)*	*Specificity (%)*
Group 1	16/30	16/30	53.33	53.33	53.33
Group 2	27/60	33/60	50.00	45.00	50.00
Group 3	53/90	33/90	48.89	58.89	49.07

Fx, fractured.

Table 8 Accuracy, sensitivity and specificity quantities of the test data for CBCT radiographs by applying multilayer perceptron neural network

CT graphics	*Fx*	*Non-fx*	*Accuracy (%)*	*Sensitivity (%)*	*Specificity (%)*
Group 1	24/30	29/30	88.33	80.00	96.00
Group 2	41/60	47/60	73.33	68.33	75.93
Group 3	63/90	54/90	65.00	70.00	63.64

Fx, fractured.

accuracy in all the three groups, was the persistence of diagnosis at an interval of changes in the variance of the network function. In this context, since there were more training data in Group 1, the variance of the results (sensitivity, specificity and accuracy of diagnosis) was almost consistent at different intervals; however, in Groups 2 and 3, the results were different with changes in the variance.

In CBCT images, the maximum persistence in terms of changes in sigma was observed in Group 1, which had greater training data. An important consideration in these radiographs is the difference in CBCT imaging technique compared with periapical radiographic technique, which resulted in 100% accuracy in detecting sound teeth by the designed neural network. Therefore, the greater the test data, the higher the accuracy, owing to the diagnosis of more sound teeth. In this context, in Group 2, the accuracy was 95%, with an accuracy of 93.33% in Group 3. In addition, the designed PNN was successful in detecting radiographs with tooth fractures, with a minimum sensitivity of 66.67% in the three groups. The CBCT images were more persistent than the periapical radiographs. In this context, in Group 3, except for $\sigma = 0.05$, the range of changes in sensitivity at different sigma values was 84.44–87.78%. However, the range of changes in sensitivity in periapical radiographs under the same conditions was 62.22–97.78%. This relative persistence in CBCT images was evident in the two other groups too.

In periapical radiographs, two factors, (1) the beam angle and (2) the distance between fractured parts, might limit the diagnosis of fracture.[21,22] If the angle of the beam is not perpendicular to the fracture path and the parts are separated minimally, the diagnosis of the fracture becomes very difficult. In many periapical radiographs, fractures with minor displacements that are not in the path of the X-ray beams might remain undetected. It can be diagnosed only based on clinical symptoms and effects on the surrounding tissues such as the formation of radiolucency in the tissues surrounding the root.

Despite the better performance of CBCT imaging rather than other digital radiographies such as periapical radiography, this technique still suffers from some important problems. In CBCT radiographs, the thinness of the fracture line, image artefacts and lack of skill on the part of the observer might lead to failure in the diagnosis of these fractures. Artefacts resulting from metallic restorative materials and the inherent artefacts of the CBCT unit might result in the obliteration of fine fracture lines. The present study was performed in laboratory conditions; so, clinical symptoms and effects on the surrounding environment are absent. The fractured parts should be separated so much so that they can be captured in radiographs.[21,22]

One of the limitations of the present study was the use of one-rooted premolar teeth. It is suggested that other teeth, such as incisors and multirooted, be used in future studies. Also, it is better to first eliminate the artefact signals (*i.e.* using the filter back-projection algorithm to reconstruct the volume data) from the image and then evaluate the radiographies with the designed neural network.

Conclusion

An efficient neural network-based model has been presented to diagnose the VRF in endodontically treated and intact teeth. Statistical results confirmed that the performance of the neural network in CBCT images is more effective than that in similar periapical radiographs. One of the major advantages of the proposed model is that it might be a useful tool for clinical applications owing to its stability in the special range of variance of functions. However, for accurate determination of success of this neural network, further *in vitro* work using a full-skull simulation for CBCT and skin/bone simulation is needed.

Our goal in future research is to study multirooted teeth for the detection of VRFs utilizing the neural network.

References

1. White S. *Oral radiology principles and interpretation*. Toronto, ON: Elsevier; 2014. p. 569.
2. Sausa S, Bortoluzzi E, Aberu M, Correa L, Correa M. Diagnostic ability of a cone beam computed tomography scan to assess longitudinal root fracture in prosthetically treated teeth. *J Endod* 2010; **36**: 1879–82.
3. Mora MA, Mol A, Tyndall DA, Rivera EM, Hill C. *In vitro* assessment of local computed tomography for the detection of longitudinal tooth fractures. *Oral Surg Oral Med Oral Pathol Oral Radiol* 2007; **103**: 825–9. doi: https://doi.org/10.1016/j.tripleo.2006.09.009
4. Nair MK, Nair UDP, Grondahl HG, Webber RL, Wallace JA. Detection of artificially induced vertical radicular fractures using tuned aperture computed tomography. *Eur J Oral Sci* 2001; **109**: 375–9.
5. Hannig C, Dullin C, Hulsmann M, Heidrich G. Three-dimensional, non-destructive visualization of vertical root fractures using flat panel volume detector computer tomography: an

ex vivo in vitro case report. *Int Endod J* 2005; **38**: 904–13. doi: https://doi.org/10.1111/j.1365-2591.2005.01033.x
6. van Daatselaar AN, van der Stelt P, Weenen J. Effect of number of projections on image quality of local CT. *Dentomaxillofac Radiol* 2004; **33**: 361–9.
7. van Daatselaar AN, Tyndall D, Verehij H, van der Stelt P. Minimum number of basis projections for caries detection with local CT. *Dentomaxillofac Radiol* 2004; **33**: 355–60. doi: https://doi.org/10.1259/dmfr/14130662
8. Lee J, Kwon K, Kol K. Diagnostic accuracy of artificially induced vertical root fracture, a comparison of direct digital periapical images with conventional periapical images. *Korean J Oral Maxillofac Radiol* 2004; **34**: 185–90.
9. Brickley MR, Shepherd JP, Armstrong RA. Neural networks: a new technique for development of decision support systems in dentistry. *J Dent* 1998; **26**: 305–9. doi: https://doi.org/10.1016/S0300-5712(97)00027-4
10. Tripathy M, Maheshwari RP, Verma HK. Power transformer differential protection based on optimal probabilistic neural network. *IEEE Trans Power Del* 2010; **25**: 102–12. doi: https://doi.org/10.1109/TPWRD.2009.2028800
11. Kositbowarnchui S, Plermkamon S, Tangkosol T. Performance of an artificial neural network for vertical root fracture detection: an *ex vivo* study. *Dent Traumatol* 2013; **29**: 151–5. doi: https://doi.org/10.1111/j.1600-9657.2012.01148.x
12. Hagan MT, Demuth R, Beale M. *Neural network design*. Boston, MA: PWS Publishing Co.; 1995.
13. Daubechies I. Orthonormal bases of compactly supported wavelets. *Commun Pure Appl Math* 1988; **69**: 909–96.
14. Bovik AC. Analysis of multichannel narrowband filters for image texture segmentation. *IEEE Trans Signal Process* 1991; **39**: 2025–43. doi: https://doi.org/10.1109/78.134435
15. Moore B. Principle component analysis in linear systems: controllability, observability, and model reduction. *IEEE Trans Autom Control* 2003; **26**: 17–32. doi: https://doi.org/10.1109/TAC.1981.1102568
16. Holst H, Mare K, Jarund A, Astrom K, Evander E, Tagil K, et al. An independent evaluation of a new method for automated interpretation on lung scintigrams using artificial neural networks. *Eur J Nucl Med Mol Imaging* 2001; **28**: 33–8.
17. Kositbowornchai S, Siriteptawee S, Plermkamon S, Bureerat S, Chetchotsak D. An artificial neural network for detection of simulated dental caries. *Int J Comput Assist Radiol Surg* 2006; **1**: 91–6. doi: https://doi.org/10.1007/s11548-006-0040-x
18. Edlund M, Nair MK, Nair UP. Detection of vertical root fractures by using cone-beam computed tomography: a clinical study. *J Endod* 2011; **37**: 768–72. doi: https://doi.org/10.1016/j.joen.2011.02.034
19. Ozer Y. Detection of vertical root fractures of different thicknesses in endodontically enlarged teeth by cone beam computed tomography *vs* digital radiography. *J Endod* 2010; **36**: 1245–9.
20. Tsesis I, Kamburoglu K, Katz A, Tamse A, Kaffe I, Kfir A. Comparison of digital with conventional radiography in detection of vertical root fractures in endodontically treated maxillary premolars: an *ex vivo* study. *Oral Surg Oral Med Oral Pathol Oral Radiol Endod* 2008; **106**: 124–8. doi: https://doi.org/10.1016/j.tripleo.2007.09.007
21. Hassan B, Metska ME, Ozok AR, van der Stelt P, Wesselink PR. Detection of vertical root fractures in endodontically treated teeth by a cone beam computed tomography scan. *J Endod* 2009; **35**: 719–22. doi: https://doi.org/10.1016/j.joen.2009.01.022
22. Melo SLS, Bortoluzzi EA, Abreu M, Correa LR, Correa M. Diagnostic ability of a cone-beam computed tomography scan to assess longitudinal root fractures in prosthetically treated teeth. *J Endod* 2010; **36**: 1879–82. doi: https://doi.org/10.1016/j.joen.2010.08.025

Appendix A

In the Gabor filter, the input image $I(x,y),(x,y)\in\Omega$ (in which Ω is a subset of the image plane) is convolved with the two-dimensional Gabor filter of $g(x,y),(x,y)\in\Omega$ as follows and the Gabor specificity function $r(x,y)$ is acquired as follows:

$$r(x,y)=\iint_{\Omega} I(\xi,\eta)g(x-\xi,y-\eta)\mathrm{d}\xi\ \mathrm{d}\eta. \qquad \text{A1}$$

In Equation (A1), the family of Gabor filters used is as follows:

$$g_{\lambda,\theta,\varphi}(x,y)=\mathrm{e}^{-\frac{x'^2+y^2y'^2}{2\sigma^2}}\times\cos\left(\frac{2\pi x'}{\lambda}+\varphi\right), \qquad \text{A2}$$

in which

$$\begin{bmatrix}x'\\y'\end{bmatrix}=\begin{bmatrix}\cos\theta & \sin\theta\\ -\sin\theta & \cos\theta\end{bmatrix}\begin{bmatrix}x\\y\end{bmatrix}. \qquad \text{A3}$$

The Gaussian function width in Equation (A2) was $\sigma=0.56\lambda$ at $\lambda=0.5$. As shown in Equation (A2), the Gabor filter is created through integration of a Gaussian function and a sine or cosine function, which results in an optimal integration of data in the two times and frequency fields, since the sine function is completely assigned to the frequency field.